IEEE Access
Multidisciplinary | Rapid Review | Open Access Journal

Received September 16, 2019, accepted October 7, 2019, date of publication October 10, 2019, date of current version October 24, 2019.

*Digital Object Identifier 10.1109/ACCESS.2019.2946855*

# A Dynamic Enhanced Robust Cubature Kalman Filter for the State Estimation of an Unmanned Autonomous Helicopter

**MIAOLEI HE, (Member, IEEE), AND JILIN HE**
The State Key Laboratory of High Performance Complex Manufacturing, Central South University, Changsha 410083, China
Corresponding authors: Miaolei He (rchml@hotmail.com) and Jilin He (hejilin@aliyun.com)

**ABSTRACT** This paper addresses a design and application for the problem of state estimation for an unmanned autonomous helicopter (UAH) equipped with instruments including an inertial measurement unit (IMU), a magnetometer and a global positioning system (GPS). A dynamic enhanced robust cubature Kalman filter (DERCKF) is proposed in this article. First, a robust filtering strategy is formulated to provide a strong constraint for abnormal values. Second, a new robust CKF is formulated based on the spherical cubature and Gaussian quadrature rules to estimate the probability state, without requiring calculation of the Jacobian and Hessian matrices. Then, an enhanced rule is proposed to help eliminate the accuracy degradation caused by model uncertainty disturbance when the experimental platform is operating and to improve the estimation performance of the filter. Meanwhile, by detecting the system uncertainty state, a dynamic enhanced strategy is formulated to achieve automatic adjustments for the dynamic enhanced robust rule and guarantee that the DERCKF will realize valid system state estimation at all times. Finally, numerical experimental results are presented to demonstrate the effectiveness and robustness of the DERCKF.

**INDEX TERMS** Cubature Kalman filter, state estimation, UAH.

## I. INTRODUCTION

Unmanned autonomous helicopters (UAHs) have the characteristics of high maneuverability, small size, low cost and vertical takeoff and landing [1], [2]. They have broad applications in areas such as industry, agriculture, and the military, and many universities and research institutes have carried out relevant research [3]–[6]. State estimation for helicopters plays a key role in UAH autonomous systems, especially for designing an autonomous system to control the helicopter safely and stably in the real world in the presence of model uncertainty [7].

The successful implementation of state estimation requires the use of rate gyros with exceptional stability and accurate information. The expensive measurement unit commonly used is accurate enough for helicopters, but it is not practical for use with UAHs due to its size, weight and cost limitations. Inexpensive units also tend to be low-performance sensors, and the navigation measurement error will accumulate significantly over time, so it is still a challenging task to adapt these instruments to long continuous flights. The traditional Kalman filter [8] was proposed to solve the estimation problem of a linear system [9], but it is not useful in this scenario. For the practical application of the Kalman filter in these nonlinear cases, many researchers have proposed some innovative approaches, which include the extended Kalman filter [10], the unscented Kalman filter [11] [12], the Gaussian filter [13], the fuzzy complementary Kalman filter [14], the sparse-grid grid quadrature filter [15], the stochastic integration filter [16] and the cubature Kalman filter [17]. Among these methods, research on the cubature Kalman filter (CKF) has attracted interest recently. Because the CKF does not require the calculation of the Jacobian and Hessian matrices, the filter is easy to create, it quickly computes estimations with low complexity, and it particularly satisfies the system requirements for fast state estimation in real time. In [18], *Benzerrouk* et al. introduced a high-degree CKF based on spherical-radial cubature rules and applied the filter in a navigation problem for an unmanned aerial vehicle (UAV). The filter was executed and verified on an AR. Drone. *Kim* et al. used a CKF to detect a multi-UAV system [19], in which a CKF-based fault detection

The associate editor coordinating the review of this manuscript and approving it for publication was Shaohua Wan.

scheme was developed to isolate the UAV fault from the flight formation, but the high-degree CKF needed substantial computing power. The H-infinity strategy was used to lower the computational burden of the CKF in [20], which can provide a strong constraint for abnormal values. Researchers in [21] used a CKF to estimate the localization-augmented state problem for a mobile robot. Due to the dynamic uncertainties of mobile platforms, the nonlinear filter performance of the position and velocity states might be severely degraded, but model uncertainty is not considered here. *Tseng* et al. proposed an adaptive CKF [22] for an integrated navigation system and utilized a fuzzy logic adaptive strategy to resolve shortcomings for selecting the process noise covariance by experience. However, their adaptive strategy is very complex, making it difficult to realize in application. Therefore, their strategy works well only in simulations and shows limited utility in real-time UAH platforms. *Hailiang* et al. proposed an adaptive method for navigation systems in a GPS-denied environment, using the strong tracking technique and the least square principle to obtain the optimal estimation when GPS data are not available [23]. The original CKF does not have strong tracking ability when the system model does not match, and system observation noise exists. It will lead to the precision decreasing and estimation results divergence. A strong tracking CKF (SCKF) was proposed to improve tracking performance in [24], with an adaptive-adjustment model that is formulated to overcome the invalidity problem of the traditional filter. However, the researchers considered only the of the state process noise and the state error, and the uncertainty of the model system was not considered. The process noise and the state error for UAHs are very difficult to identify, with the characteristics of uncertainty and high compiling. This disadvantage limited the filter performance. Researchers in [25] used the strong tracking method to improve the CKF tracking performance when a target makes abrupt state changes. However, the strong tracking strategy was conventional, which limits the application to UAHs. The algorithms in [26], [27] are so complicated that it is challenging to use them with UAHs, and the algorithms have been verified only in simulations. *Jianwang* et al. proposed a Bayesian-based strong tracking interpolatory CKF method to improve the traditional CKF performance in target tracking [28] in simulations, but the fading factor exists during the entire filtering process, and system uncertainty is not considered in the process. These disadvantages make it difficult to implement these algorithms with UAHs, for which uncertainty appears randomly during the entire process.

According to the authors' knowledge, a state estimation system based on this kind of CKF has not yet been investigated in the UAH community. In the traditional CKF process, the previous state is involved in estimating the current system state directly. In contrast to the conventional process, an intelligent way of using the previous estimation information is discussed. Hence, to overcome the problems of the conventional filters and to improve the state estimation performance, we propose a dynamic enhanced robust cubature Kalman filter (DERCKF) combined with a robust strategy and a dynamic enhanced CKF.

The main contributions of this paper are as follows. First, a robust strategy is proposed that can provide a strong constraint for abnormal values, and the novel CKF algorithm has the ability to realize an improved state estimation performance for UAHs. Second, an enhanced CKF algorithm is proposed to help improve the estimation performance of the proposed CKF when the experimental platform is operating in the existence of disturbances. A novel computing fading factor algorithm is described in detail without Jacobian and Hessian matrix calculations, saving execution time. Third, a dynamic enhanced strategy is proposed to achieve automatic adjustment of the enhanced strategy by detecting the system uncertainty state, and in this way, the DERCKF achieves valid system state estimation in due course and avoids the loss of accuracy when system uncertainty does not exist. Finally, comparable experimental results are given to verify the higher robustness and accuracy of proposed method compared to other CKF algorithms—not in simulations but on a real helicopter platform.

## II. SYSTEM AND MEASUREMENT MODELS

### A. SYSTEM MODEL

The UAH navigation system utilizes a loose coupling model of the IMU and GPS. In this paper, the IMU/GPS measurement model uses the following assumptions: the position, velocity and attitude information from the GPS are included in the model; the horizontal angle error is small and can be ignored; and the drift error consists of the one-order Markova component and a constant value.

The gyroscope output in the body coordinate system is

$$g_{b(t)} = \left[\, \omega_{bx(t)} \;\; \omega_{by(t)} \;\; \omega_{bz(t)} \,\right]^{\mathrm{T}} \tag{1}$$

However, the real output contains different errors and cannot be observed ideally according to Eq. 1. The real output should be rewritten as

$$\tilde{\omega}_{b(t)} = g_{b(t)} - \delta_{\omega_b(t)} \tag{2}$$

where $\delta_{\omega_b(t)}$ is the gyroscope measurement error.

$$\delta_{\omega_b(t)} = \left[\, \delta_{\omega_{bx}(t)} \;\; \delta_{\omega_{by}(t)} \;\; \delta_{\omega_{bz}(t)} \,\right]^{T} \tag{3}$$

Similarly, we can obtain the accelerometer and magnetometer output expressions as

$$\begin{cases} \tilde{a}_{b(t)} = a_{b(t)} - \delta_{a_b(t)} \\ \tilde{m}_{b(t)} = m_{b(t)} - \delta_{m_b(t)} \end{cases} \tag{4}$$

The measurement errors are

$$\begin{cases} \delta_{a_b(t)} = \left[\delta_{a_{bx}(t)} \quad \delta_{a_{by}(t)} \quad \delta_{a_{bz}(t)}\right]^{T} \\ \delta_{a_b(t)} = \left[\delta_{m_{bx}(t)} \quad \delta_{m_{by}(t)} \quad \delta_{m_{bz}(t)}\right]^{T} \end{cases} \tag{5}$$

Here, to overcome the singular problem in the attitude calculation, the attitude quaternion algorithm is used to update the attitude information process. After the discretization process, the attitude matrix $\Psi_{n,k}$ and velocity matrix $\mathrm{V}_{n,k}$

expressions of the UAH in the local north-east-down (NED) coordinate system can be expressed as

$$\Psi_{n,k} = \Psi_{n,k-1} + \mathrm{R}_{k-1}\tilde{\omega}_{b,k}\Delta \mathrm{t} \tag{6}$$
$$\mathrm{V}_{n,k} = \mathrm{V}_{n,k-1} - \mathrm{R}_{b-e,k-1}\tilde{a}_{b,k}\Delta t \tag{7}$$

The position expression in the NED coordinate system is

$$\mathrm{P}_{n,k}=\mathrm{P}_{n,k-1} - \mathrm{V}_{n,k}\Delta t \tag{8}$$

where $\mathrm{R}_{k-1}$ and $\mathrm{R}_{b-e,k-1}$ are the rotation matrices defined in [6]. In general, Eq. 6-8 are the system model.

### B. MEASUREMENT SYSTEM MODEL

The measurement model in the previous section can be rewritten as

$$\begin{cases} X_{k+1} = f(X_k) + V_k \\ Y_k = HX_k + N_k \end{cases} \tag{9}$$

where $X_k = [\Delta r_k^e, \Delta \dot{r}_k^e, q_{k,m}, \Delta gyr_k^b, \Delta a_{k,b}, \Delta atti_k]^T$, $m$=*0,1,2,3* is the state vector of the system; $\Delta r_k^e$ and $\Delta \dot{r}_k^e$ are the position and velocity errors, respectively, and both are in the NED coordinate system; $q_{k,m}, m = 0, 1, 2, 3$ is the quaternion of the attitude angle; $\Delta gyr_k^b$ and $\Delta a_{k,b}$ are the gyroscope and accelerometer drift error, respectively, and $\Delta atti_k$ is the attitude error, all of which are in the body coordinate system; $f(*)$ is the system dynamic function; $Y_k = \left[\Delta_{k,ned}, \Delta_{k,v}, a_{k,b}, m_{k,b}\right]$ is the measurement vector of the system; $\Delta_{k,ned}$ and $\Delta_{k,v}$ are the position and velocity difference value vectors, respectively, of the IMU calculation and GPS measurement, both of which are in the conventional terrestrial system; $a_{k,b}$ is the component of the accelerometer, $m_{k,b}$ is the component of the magnetometer, and both are in the body coordinate system; $V_{k-1}$ and $N_k$ are the process error and measurement noise, respectively. We can also obtain the observation matrix $H$ when the measurement and state are in the same coordinate system:

$$H = \begin{bmatrix} I_{3\times3} & 0_{3\times3} & 0_{3\times4} & 0_{3\times9} \\ 0_{3\times3} & I_{3\times3} & 0_{3\times4} & 0_{3\times9} \\ 0_{6\times3} & 0_{6\times3} & Quat_{6\times4} & 0_{6\times9} \end{bmatrix} \tag{10}$$

where $Quat_{6\times4}$ is the linearized transfer matrix of $a_{k,b}$ and $m_{k,b}$ composed of the quaternion $q_{k,m}, m = 0, 1, 2, 3$. Because the attitude solution algorithm is not the focus of the present study, readers interested in this part can refer to [29]. Here, the initial quaternion value is $q_{0,m} = [1\ 0\ 0\ 0]$.

## III. DYNAMIC ENHANCED ROBUST CKF DESIGN

The DERCKF is proposed in this section. The filtering process of the DERCKF is shown in Fig. 1. The robust $\mathrm{H}_\infty$ norm principle is introduced to overcome the abnormal observed value first. Additionally, a CKF technique is incorporated to estimate the system state. To enhance the filter dynamic estimation performance, an enhanced strategy is used in the CKF. Also, it is reasonable for us to formulate a dynamic detection algorithm to determine that the enhanced CKF algorithm can be introduced into the filter in due course. In this way, we can avoid a loss of accuracy when system uncertainty does not exist.

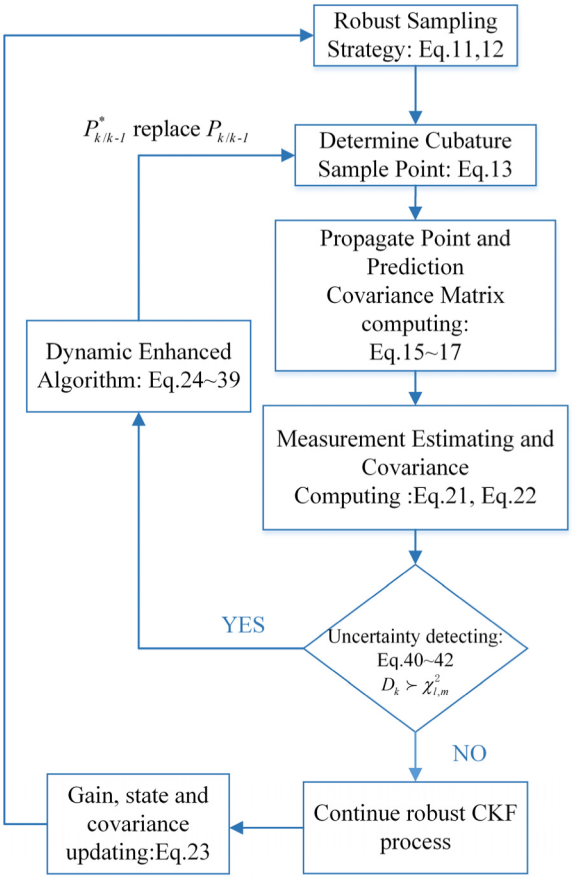


**FIGURE 1.** Filtering process of the DERCKF.

The key point is that the previous state information at time *k-1* is utilized to estimate the system state information at time *k*. Thus, a dynamic enhanced rule is introduced to extract useful information from a previous estimation state to enhance the current estimation performance. A dynamic enhanced strategy is designed to guarantee that the enhanced rule is injected into the process when the system state meets the enhanced decision criteria by detecting the system uncertainty state.

### A. ROBUST CKF ALGORITHM

The robust $\mathrm{H}_\infty$ norm principle is introduced to resolve abnormal measurement values. The transfer function norm of the noise input to the estimation error output is expected to be less than a constraint value $\gamma$. The cost function is given by

$$J = \frac{\sum_{k=1}^{N} \left\| X_k - \hat{X}_k \right\|}{\left\| X_0 - \hat{X}_0 \right\|^2_{P_0^{-1}} + \sum_{k=1}^{N} \left( \| V_k \|^2_{Q_k^{-1}} + \| N_k \|_{R_k^{-1}} \right)} < \gamma \tag{11}$$

where $\hat{X}_k$ is the estimated value of discrete state variant $X_k$ at time$k$; $\gamma$is the threshold value, which meets the Riccati inequality $P_k^{-1} + H_k^T H_k - \gamma^{-2} L_k^T L_k > 0$; $\hat{X}_0$ is the

estimation of $\left\|X_0-\hat{X}_0\right\|^2_{P_0^{-1}}(X_0-\hat{X}_0)^T P_0^{-1}(X_0-\hat{X}_0)$; $X_0$ is the initial state of the system; and $P_0$ is the variance of $X_0$. The probability density functions are represented by $P_{(V_k)} = N(V_K; 0, Q_k)$ and $P_{(N_k)} = N(N_k; 0, R_k)$, wherein $Q_k$ and $R_k$ are the covariance matrices of the system:

$$\begin{cases} P_k = P_{k|k-1} - \begin{bmatrix} P_{XY,k} & P_{k|k-1} \end{bmatrix} P_\gamma \begin{bmatrix} P_{XY,k} & P_{k|k-1} \end{bmatrix}^T \\ P_\gamma = \begin{pmatrix} P_{YY,k} - P_k + I & P_{XY,k}^T \\ P_{XY,k} & P_{k|k-1} - \gamma^2 \mathrm{I} \end{pmatrix} \end{cases} \tag{12}$$

where $L_k$ is the restraint matrix and $H_k$ is the measurement matrix. $\gamma$ is related to the robustness degree of the estimation system. There is not enough space here to do discuss the richness of the calculation process. Readers interested in its derivation can refer to [30].

The steps of the robust CKF are as follows:

*Step 1*: Determine the cubature sample point.

The cubature points $\gamma_i$ and the corresponding weights $w_i$ are given by

$$\gamma_i = \begin{cases} \sqrt{\mathrm{n}}e_i, i=1,...,n \\ -\sqrt{\mathrm{n}}e_i, i = n+1,...,2n \end{cases} \tag{13}$$

$$W_i = \frac{1}{2n}, i = 1, ..., 2n \tag{14}$$

where $i$ is the number of the cubature sample point.

*Step 2*: Information prediction.

The robust strategy easily leads to the lack of a solution to the Riccati inequality and the divergence of the filter, which make the strategy unsuitable for application on a real helicopter. To overcome this issue, we use the singular value decomposition method to guarantee the symmetric nonnegative definite characteristic of the covariance matrix $P_{k-1}$, implement it, and then place the Cholesky decomposition in the $\mathrm{H}_\infty$CKF. That is, $P_{k-1} = U_{k-1}S_{k-1}V_{k-1}^T$, where $S_{k-1}$ is a diagonal matrix. The propagated CKF point can be calculated by

$$X'_{\mathrm{i},k-1} = U_{i,k-1}S_{k-1}\gamma_\mathrm{i} + \hat{X}_{k-1} \tag{15}$$

where $S_{k-1}$ is the square root matrix of $P_{k-1}$:

$$S_{k-1} = \sqrt{P_{k-1}} \tag{16}$$

Through using this method, the calculation process achieves better numerical stability. In addition, the filter can achieve more robust results for a wider range of parameter conditions. The prediction covariance matrix can be calculated by

$$\begin{aligned} P_{k|k-1} = &\sum_{i=1}^{N} W_i \left(f\left(X'_{i,k-1}\right) - \hat{X}_{k-1}\right) \\ &\left(f\left(X'_{i,k-1}\right) + \hat{X}_{k-1}\right)^{\mathrm{T}} + \mathrm{Q}_{k-1} \end{aligned} \tag{17}$$

where $N$ is the number of points. The estimation information is

$$\hat{X}_{k|k-1} = \sum_{i=1}^{N} W_i f\left(X'_{i,k-1}\right) \tag{18}$$

where $W_i$ is the filter coefficient value at point$i$.

*Step 3*: Measurement updating.

The state at time $k$ is given by

$$X_{i,k|k-1} = S_{\mathrm{k}-1|k-1}\gamma_\mathrm{i} + X_{k|k-1} \tag{19}$$

The measurement information at time$k$ is given by

$$Y_{i,k|k-1} = H\left(X_{k|k-1}\right) \tag{20}$$

The measurement estimation process can be expressed as

$$\hat{Y}_k = \sum_{\mathrm{i}=1}^{N} W_\mathrm{i} Y_{i,k|k-1} \tag{21}$$

The cross variance and covariance can be given by

$$\begin{cases} P_{XY,k} = \sum_{\mathrm{i}=1}^{N} W_\mathrm{i}\left(X'_{\mathrm{i},k-1} - \hat{x}_{k-1}\right)\left(H\left(X'_{\mathrm{i},k-1}\right) - \hat{Y}_{k-1}\right)^{\mathrm{T}} \\ P_{YY,k} = \sum_{\mathrm{i}=1}^{N} W_\mathrm{i}\left(\mathrm{H}\left(X'_{\mathrm{i},k-1}\right) - \hat{Y}_{k-1}\right) \\ \qquad \left(H\left(X'_{\mathrm{i},k-1}\right) - \hat{Y}_{k-1}\right)^{\mathrm{T}} \end{cases} \tag{22}$$

The state and covariance updating equations are given by

$$\begin{cases} \hat{X}_k = \bar{X}_k + K_k\left(\mathrm{Y}_k - \hat{Y}_k\right) \\ P_k = P_{k|k-1} - K_k P_{zz,k} K_k^T \end{cases} \tag{23}$$

where the gain matrix $K_k = P_{XY,k}/P_{YY,k}$.

A robust filtering strategy is formulated to provide a strong constraint for abnormal values. Then, a robust CKF is formulated using the spherical cubature and Gaussian quadrature rules to estimate the probability state. This makes the linearization of the nonlinear measurement function lose less accuracy than in the traditional method. Because the CKF does not require the Taylor series approximation of the nonlinear function, which makes it possible to estimate the system state without calculation of the Jacobian and Hessian matrices, it saves execution time. Finally, the singular value decomposition method is introduced to overcome the singular problem in the computing process. All these attributes make the filter more robust and the system easy to implement on a real unmanned helicopter platform.

### B. AN ENHANCED CKF ALGORITHM

In this section, an enhanced strategy is introduced into the robust CKF process. Regarding the problem of nonlinear UAH state estimation, the traditional enhanced algorithm requires the Jacobian calculation of the measurement system, which limits the practical applications of the traditional Kalman filter. The enhanced factor exists in the entire filtering process, which cannot guarantee that the filter operation will always maintain an optimal estimation. Therefore, it is difficult to achieve accurate estimations at all times when the CKF is implemented on a real helicopter, wherein model uncertainty exists. The enhanced concept utilizes the structure of a long-term state to improve the estimation performance. In practical terms, a forgetting factor is introduced to extract useful information from the previous estimation state and to adjust the gain matrix in real time, depending on the different cases of the system model.

Based on the enhanced strategy, a novel prediction covariance matrix in Eq. (17) can be constructed as

$$P^*_{k|k-1} = \lambda_{\mathrm{k}} \left\{ \begin{array}{l} \sum_{i=1}^{N} W_{\mathrm{i}} \left( f\left(X'_{i,k-1}\right) - \hat{X}_{k-1} \right) \cdot \\ \left( f\left(X'_{i,k-1}\right) + \hat{X}_{k-1} \right)^{\mathrm{T}} + \mathrm{Q}_{k-1} \end{array} \right\} \tag{24}$$

where $\lambda_{\mathrm{k}}$ is the enhanced factor, which can be obtained from the following equation

$$\begin{cases} E_{\min}\left[(X_k - \hat{X}_k)(X_k - \hat{X}_k)^T\right] \\ E\left[(Y_k - \hat{Y}_{k|k-1})^T (Y_{k+j} - \hat{Y}_{k+j|k+j-1})\right] = 0 \end{cases} \tag{25}$$

The first line in Eq. 25 is the performance index of the filter. The second line can ensure that the new state vector sacrifices the orthogonality relation, which has the ability to guarantee that the effective information has been extracted and determine whether the filter performance is excellent. Thus, the key point is the determination of the value $\lambda_k$.

We define the estimation error and prediction error as

$$\begin{cases} \tilde{X}_k = X_k - \hat{X}_k \\ \tilde{X}_{k|k-1} = X_k - \hat{X}_{k|k-1} \end{cases} \tag{26}$$

By substituting Eq. 10 into Eq. 26, we can rewrite the prediction error as

$$\tilde{X}_{k|k-1} = F_k \cdot X_k + \Delta(\tilde{X}_{k-1}) + \mathrm{V}_k \tag{27}$$

where $F_k = \left.\frac{\partial f(X)}{\partial (X)}\right|_{X=\hat{X}_{k-1}}$ and $\Delta(\tilde{X}_{k-1})$ is the second and upper-order matrix in the Taylor expansion. Cause the Taylor expansion will produce an inevitable error in the linearization process. In order to build the standard state estimation equation and better describe the error of the first-order linearization approximation, an unknown time-varying-diagonal matrix is introduced

$$\beta_k = \mathrm{diag}(\beta_{1,k},...,\beta_{n,k}) \tag{28}$$

Then, by substituting this expression into Eq. 27, we can obtain

$$\tilde{X}_{k|k-1} = \beta_k F_k \tilde{X}_{k-1} + V_k \tag{29}$$

Similarly, a new innovation can be obtained:

$$\begin{cases} Y_k = a_k H \tilde{X}_{k|k-1} + N_k \\ \alpha_k = \mathrm{diag}(\alpha_{1,k},...,\alpha_{n,k}) \end{cases} \tag{30}$$

The new cross variance and covariance can be rewritten as

$$\begin{cases} \hat{P}_{\hat{Y}_{k|k-1}} = E\left[(Y_k - \hat{Y}_{k|k-1})(Y_k - \hat{Y}_{k|k-1})^T\right] \\ \qquad = a_k H \hat{P}_{k|k-1} H^T a_k + N_k \\ \hat{P}_{\hat{X}_{k|k-1},\hat{Y}_{k|k-1}} = E\left[(X_k - \hat{X}_{k|k-1})(Y_k - \hat{Y}_{k|k-1})^T\right] \\ \qquad = \hat{P}_{k|k-1} H^T a_k \end{cases} \tag{31}$$

By combining Eq. 29-30, we can obtain

$$\tilde{Y}_k = \alpha_k H(\beta_k F_k \tilde{X}_{k-1} + V_k) + N_k \tag{32}$$

Upon defining $M_{j,k} = E\left[\tilde{Y}_{k+j}\tilde{Y}_k^T\right]$, it is easy to prove that

$$\begin{aligned} M_{j,k} &= E\left[\tilde{Y}_{k+j}\tilde{Y}_k^T\right] \\ &= E\{[\alpha_{k+j}H(\beta_{k+j}F_{k+j}\tilde{X}_{k+j-1} + V_{k+j}) + N_{k+j}] \\ &\quad \times [\alpha_k H(\beta_k F_k \tilde{X}_{k-1} + V_k) + N_k]^T\} \\ &= \alpha_{k+j} H \beta_{k+j} F_{k+j} \cdot [\prod_{i=k+1}^{k+j-1} (I - K_i \alpha_i H_i)\beta_i F_i] \\ &\quad (\hat{P}_{\hat{X}_{k|k-1},\hat{Y}_{k|k-1}} - K_k M_{o,k}) \end{aligned} \tag{33}$$

where $M_{o,k}$ can be calculated by

$$M_{o,k} = \begin{cases} \tilde{Y}_1 \tilde{Y}_1^T, k = 1 \\ \dfrac{v_{enh} M_{o,k-1} + \tilde{Y}_k \tilde{Y}_k^T}{1 + v_{enh}}, k \geq 2 \end{cases} \tag{34}$$

where $v_{enh}$ is the forgetting coefficient for $v_{enh} \in (0, 1)$. When Eq. 33 satisfies $M_{j,k} = 0$, we can obtain

$$\hat{P}_{\hat{X}_{k|k-1},\hat{Y}_{k|k-1}} - K_k M_{o,k} = 0 \tag{35}$$

Substituting the improved covariance matrix Eq. 24 into Eq. 31 and replacing $\hat{P}_{k|k-1}$ with $P^*_{k/k-1}$ gives a new cross covariance and a new measurement covariance:

$$\begin{cases} \hat{P}^*_{\hat{X}_{k|k-1},\hat{Y}_{k|k-1}} = P^*_{k/k-1} H^T \alpha \\ \qquad = \lambda_k \hat{P}_{k|k-1} H^T \alpha_k \\ \hat{P}^*_{\hat{Y}_{k|k-1}} = \alpha_k H P^*_{k/k-1} H^T \alpha_k + N_{\mathrm{k}} \\ \qquad = \lambda_k \alpha_k H \hat{P}_{k|k-1} H^T \alpha_k + N_{\mathrm{k}} \end{cases} \tag{36}$$

The gain matrix $K_k$ can be rewritten as $K_k = \hat{P}^*_{\hat{X}_{k|k-1},\hat{Y}_{k|k-1}} \Big/ \hat{P}^*_{\hat{Y}_{k|k-1}}$. Eq. 35-36 subsequently yield the enhanced coefficient equation as follows

$$\begin{aligned} M_{o,k} - N_k &= \hat{P}^*_{X_{k|\hat{k-1}},\hat{Y}_{k|k-1}} K_k^{-1} - N_k \\ &= \hat{P}^*_{\hat{X}_{k|k-1},\hat{Y}_{k|k-1}} \hat{P}^*_{Y_{k|\hat{k-1}}} \hat{P}^{*-1}_{X_{k|\hat{k-1}},\hat{Y}_{k|k-1}} - N_k \\ &= \hat{P}^*_{Y_{k|\hat{k-1}}} - N_k \\ &= \lambda_k \alpha_k H \hat{P}_{k|k-1} H^T \alpha_k \\ &= \lambda_k (\hat{P}_{Y_{k|\hat{k-1}}} - N_{\mathrm{k}}) \\ &= \lambda_k \sum_{i=1}^{N} W_{\mathrm{i}} \left(\gamma_{i,k|k-1} - \hat{Y}_{k|k-1}\right) \\ &\quad \left(\gamma_{i,k|k-1} - \hat{Y}_{k|k-1}\right)^{\mathrm{T}} \end{aligned} \tag{37}$$

The matrix trace operation is carried out on Eq. 37 to yield the enhanced coefficient $\lambda_k^*$

$$\lambda_k^* = \frac{Tr(M_{o,k} - N_k)}{Tr\left(\sum_{i=1}^{N} W_{\mathrm{i}} \left(\gamma_{i,k|k-1} - \hat{Y}_{k|k-1}\right)\left(\gamma_{i,k|k-1} - \hat{Y}_{k|k-1}\right)^{\mathrm{T}}\right)} \tag{38}$$

When using this equation to calculate $\lambda_k$, the value will be less than 1 in some cases. To ensure that $\lambda_k$ is always greater than 1 in the filtering process, we determine the value by

$$\lambda_k = \max(1, \lambda_k^*) \tag{39}$$

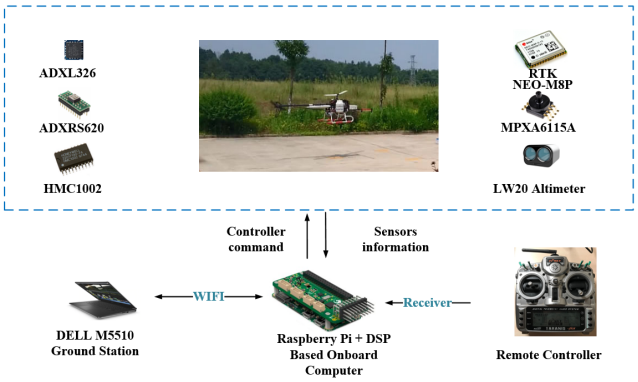


**FIGURE 2.** The experimental helicopter.

### C. DYNAMIC ENHANCED STRATEGY

As mentioned earlier, it is obvious that the DERCKF does not need to compute the system Jacob matrix when solving for $\lambda_k$. The advantages of the dynamic enhanced method can guarantee more accurate state estimation results when the measurement system model is uncertain in some scenarios. The improved covariance matrix in Eq. 24 is the dynamic enhanced factor when model uncertainty exists. Therefore, it is reasonable for us to formulate an uncertainty feature detection algorithm to determine that the enhanced CKF algorithm can be introduced into the filter in due course. In this way, we can avoid a loss of accuracy when system uncertainty does not exist. The uncertainty detection index is designed as

$$\begin{aligned} D_k &= \tilde{Y}_k^T \cdot P_{\hat{z}_{k|k-1}}^{-1} \cdot \tilde{Y}_k \\ &= \tilde{Y}_k^T \left\{ \sum_{i=1}^{N} W_{\mathrm{i}} \left( \gamma_{i,k|k-1} - \hat{Y}_{k|k-1} \right) \right. \\ &\qquad \left. \left( \gamma_{i,k|k-1} - \hat{Y}_{k|k-1} \right)^{\mathrm{T}} \right\}^{-1} \tilde{Y}_k \end{aligned} \tag{40}$$

We define two assumption scenarios for the estimation system:

Case 1 $C_0$: The estimation system works normally.

Case 2 $C_1$: The estimation system contains model uncertainty.

Meanwhile, the detection index $D_k$ always strictly obeys the $\chi^2$ distribution of $m$ degrees of freedom. The significance level $l \in (0, 1)$ can be used to determine the gate value $\chi^2_{l,m}$ by

$$P(\chi^2 \succ \chi^2_{l,m}) = l \tag{41}$$

The dynamic enhanced method is used in the estimation system only if the assumed condition is valid, that is, if $D_k$ is greater than $\chi^2_{l,m}$. This process can be expressed as $D_k \succ \chi^2_{l,m}$, with $P^*_{k/k-1}$ replacing $P_{k/k-1}$:

$$\begin{aligned} C_0 &: D_k \leq \chi^2_{l,m}, \forall k \\ C_1 &: D_k \succ \chi^2_{l,m}, \exists k \end{aligned} \tag{42}$$

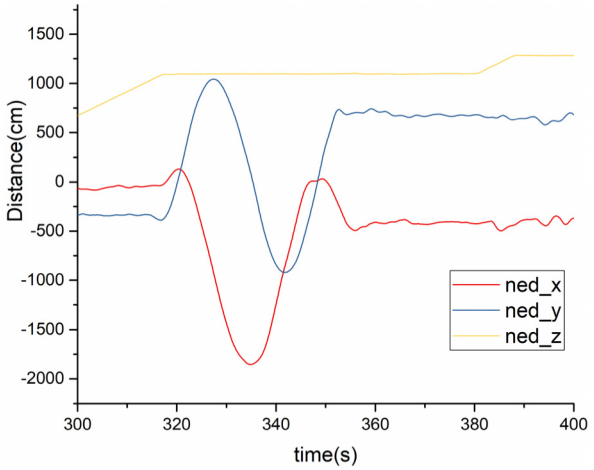


**FIGURE 3.** The pirouetting flight path.

## IV. EXPERIMENT

### A. PLATFORM

To verify the effectiveness of the proposed DERCKF, an estimation performance experiment on a real UAH is conducted. The small helicopter is equipped with an onboard computer with Raspberry Pi, an accelerometer (ADXL326), a gyroscope (ADXRS620), a magnetometer (HMC1002), an altimeter (MPXA6115A+LW20), and a real-time kinematic GPS (RTK NEO-M8P), as shown in Fig. 2. The measurement accuracy of velocity is 1 cm/s, that of the attitude is 0.1 degree, and that of the position is 1 cm. The LiDAR module LW20, which is mounted downward, can measure heights in the range of 0∼110.00 m, with a resolution of 1 cm. The barometer will be used in the height measurement process when the platform height exceeds the LiDAR range. To record the flight data, a data recording system is designed on the embedded platform using a memory card. For the DERCKF performance test, a pirouetting flight motion under model uncertainty is selected to obtain the original data, and the mission path is shown in Fig. 3. We adapt the real helicopter in Fig. 2 to compare the performances of the traditional CKF, the SCKF [24] and the DERCKF. The weight of the UAH in Fig. 2 is 9.6 kilograms, and the main rotor radius is 0.82 m. Meanwhile, a high-precision measurement ADIS 16488CMLZ is used in the platform to acquire the accuracy measurement data, which is also recorded on the memory card. The different characteristics of the sensors are shown in Table 1. The two sets of measurement are presented in the same place to guarantee that the units are operating under the same conditions.

### B. EXPERIMENTAL RESULTS

The helicopter takes off from a table at a safe speed of 2.5 m/s and then flies to the preset point: $(-25cm, -380cm, 1100cm)$. The helicopter then executes a pirouetting flight mission. The overall flight process takes 200 seconds, and the path is shown in Fig. 3. The wind speed is approximately 6 m/s.

**TABLE 1.** Main parameters of the sensor module.

| Sensor | ADXL326 | ADXRS620 | HMC1002 | ADIS 16488CMLZ | |
|---|---|---|---|---|---|
| parameters | acc. | gyr. | mag. | acc. | gyr. |
| Measured nonlinearity (%) | ±0.3 | ±0.1 | ±0.1 | ±0.1 | ±0.1 |
| Noisy density ($Hz^{-0.5}$) | 300 *mg* | 0.05 ° | 1.8 *mGauss* | 63 *mg* | 0.0059 ° |
| Measurement range | ±19 g | ±300 ° | ±2 Gauss | ±18 g | ±450 ° |

*acc. for accelerometer, gyr. for gyroscope, mag. for magnetometer.

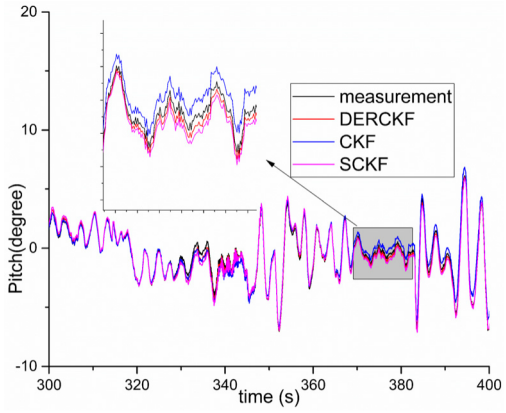


**FIGURE 4.** The attitude responses of the pitch channel.

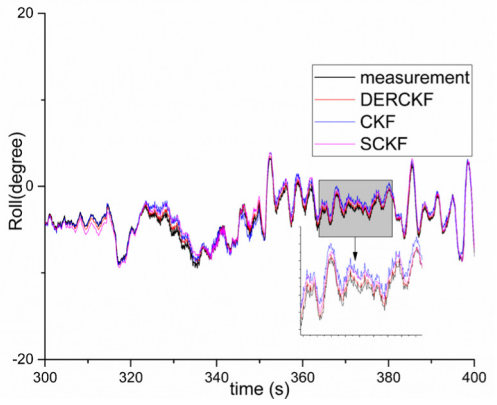


**FIGURE 5.** The attitude responses of the roll channel.

During this experiment, a measured pirouetting flight mission is performed as a test to compare the performances of the different filters. The attitude response curves are shown in Fig. 4–6. From the performance of the pitch, roll and yaw channels, it is possible to compare the attitude estimation performances of the filters. The original CKF is the least-accurate filter in estimating the UAH state, followed by the SCKF [24] and the DERCKF. The latter two filters show similar accuracy estimation abilities. However, the proposed DERCKF is the best filter, and it obtains values closest to the measured states. It seems that the filters have clear differences, and the estimated performances of the three filters are acceptable for the platform. As shown in the zoomed area, the DERCKF performance is significantly better than those of the other filters. In the yaw channel response performance

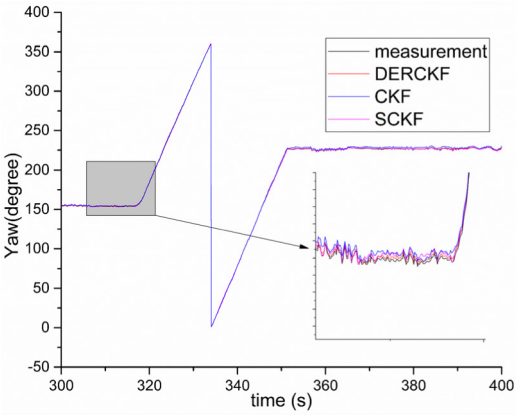


**FIGURE 6.** The attitude responses of the yaw channel.

in Fig. 6, the estimation error of the traditional CKF accumulates at the beginning and yields an error space in the measurement curve in the process. Both the SCKF and the DERCKF are more accurate than the traditional CKF, but the proposed filter is still the best, producing the least error. Additionally, it can be observed that strong coupling exists between the pitch and the yaw channel. Thus, accurately estimating the state is a very challenging task.

To better verify the DERCKF performance, the error distribution drawings of the attitude are shown in Fig. 7 for 1000 even distribution sampling points, by using the estimation results to subtract the measurement ones. In the roll channel, the CKF error is distributed from $-2.4°$ to $1.6°$ the SCKF is distributed from $-1.6°$ to $1.3°$, and the DERCKF is distributed from $-0.8°$ to $0.7°$. For the CKF, the SCKF, and the DERCKF, the error distribution between $(-1°,1°)$ accounted for 83.6%, 86.3%, and 100%, respectively, of the total. In the pitch error histograms for the CKF, the SCKF, and the DERCKF, the error distribution between $(-0.5°,0.5°)$ accounted for 69.3%, 63.3%, and 91.9%, respectively, of the total. In the yaw channel, the CKF estimation error distribution is clearly more decentralized than those of the other two filters. The CKF error range is from $-2.6°$ to $1.4°$, while for the SCKF and the DERCKF, the error distribution between $(-0.5°,0.5°)$ accounted for 62.9% and 91.9%, respectively, of the total. By comparing the error histograms of the three filters in Fig. 7, it can be found that the estimation performance of the proposed DERCKF is better than that the SCKF and CKF in terms of both the error range and the distribution.

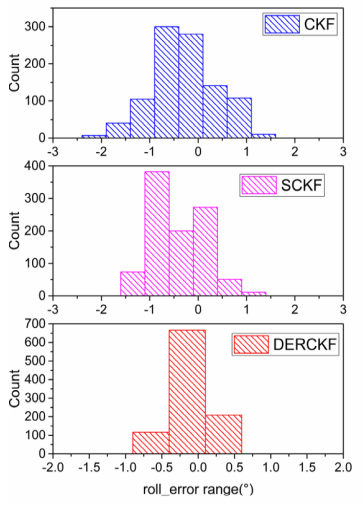


a. Roll error

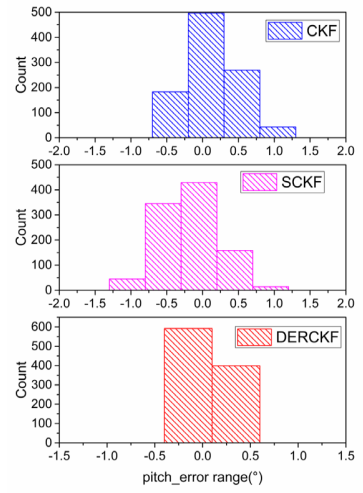


b. Pitch error

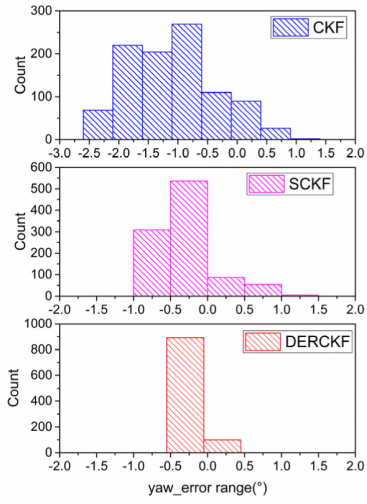


c. Yaw error

**FIGURE 7.** The error histograms of the attitude response.

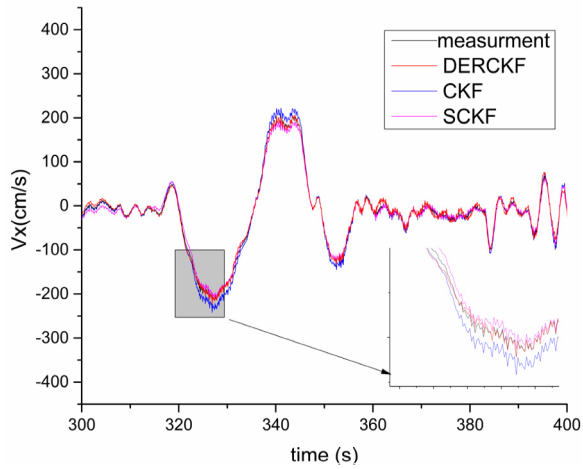


**FIGURE 8.** The velocity responses of the *Vx* channel.

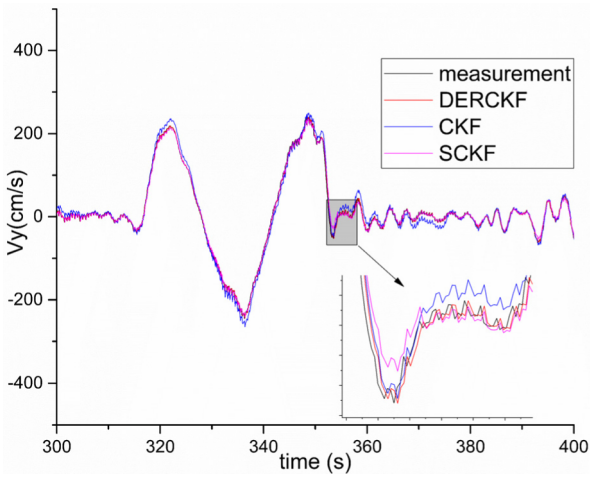


**FIGURE 9.** The velocity responses of the *Vy* channel.

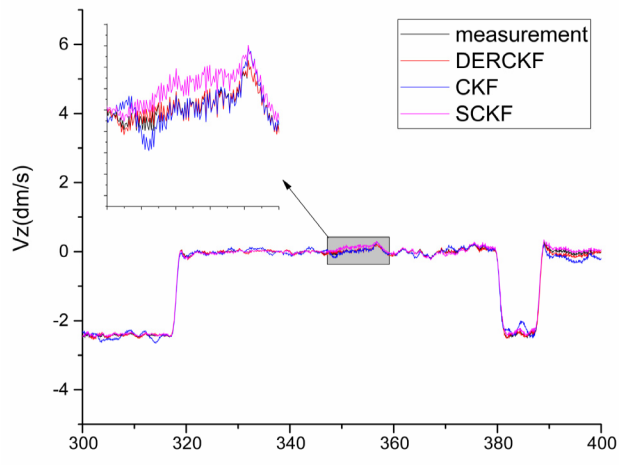


**FIGURE 10.** The velocity esponses of the *Vz* channel.

The velocity response curves are shown in Fig. 8–10. From the performance of the *Vx*, *Vy*, and *Vz* channels, it is easy to observe the comparative performances of the filters in velocity estimation. The proposed DERCKF achieves the best velocity estimation performance, and its values are the closest to those of the measured curve. Additionally, we can see that the vertical speed is much more stable than the *x* and *y* coordinate speeds.

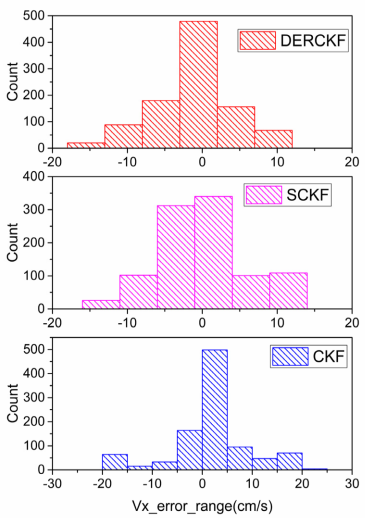


a. V$x$ error

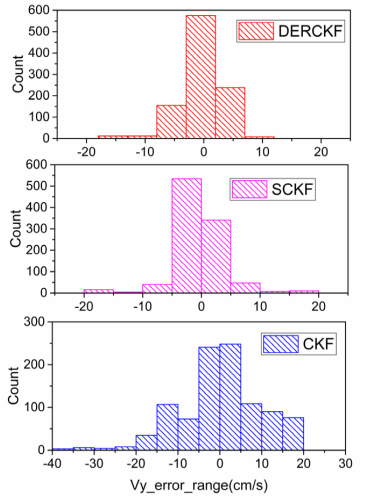


b. V$y$ error

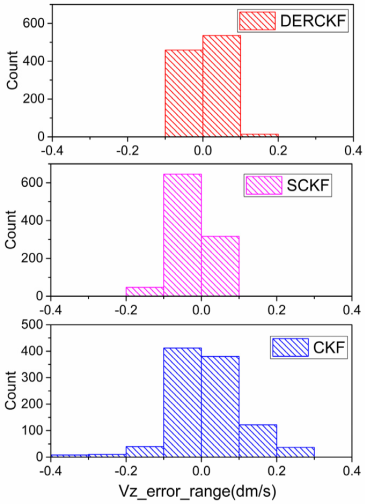


c. V$z$ error

**FIGURE 11.** The error histograms of the velocity responses.

The error distribution drawings of the velocity are shown in Fig. 11. For the V$x$ channel, the CKF, SCKF, and DERCKF errors are distributed from −20 cm/s to 25 cm/s, from −16 cm/s to 14 cm/s, and from −17 cm/s to 12 cm/s, respectively. For the V$y$ channel, the CKF, SCKF, and DERCKF errors range from −40 cm/s to 20 cm/s, from −20 cm/s to 20 cm/s, and from −18 cm/s to 12 cm/s, respectively, and the error distribution between −10 cm/s and 10 cm/s accounts for 95.1%, 93.0% and 80.2%, respectively, of the total. For the V$z$channel, the CKF, SCKF, and DERCKF errors range from −0.4 dm/s to 0.3 dm/s, from −0.2 dm/s to 0.1 dm/s, and from −0.1 dm/s to 0.2 dm/s, respectively, and the error between −0.1 dm/s and 0.1 dm/s accounts for 98.6%, 95.3% and 78.5%, respectively, of the total. As illustrated in Fig. 10, the filtering errors of the three algorithms are located near the zero line. However, comparatively speaking, the total error range of the proposed method is the least, and the error distribution is the most concentrated. These comparative results prove that the proposed DERCKF is effective. Meanwhile, the computational cost of the proposed method is approximately 4.8 ms, which is a little longer than those of the SCK and CKF. However, it still meets the real-time requirements of the UAH platform.

## V. CONCLUSION

To solve the UAH state estimation problem, a novel dynamic enhanced robust cubature Kalman filter (DERCKF) is proposed to improve the filter accuracy of the UAH state estimation system, which greatly impacts the performance of autonomous helicopters. First, the IMU/GPS model is analyzed. The DERCK algorithm is described in detail. Then, a system uncertainty detection method is proposed to achieve automatic adjustments of the enhanced rule. To evaluate the performance of the filter, attitude and velocity state estimation tests are conducted on an experimental helicopter. Based on a series of comparisons, the results show that the DERCKF has a better ability to achieve accurate state estimation than traditional methods and offers a clear advantage for use in UAH applications.

## REFERENCES

[1] B. Zhou, Z. Li, Z. Zheng, and S. Tang, "Nonlinear adaptive tracking control for a small-scale unmanned helicopter using a learning algorithm with the least parameters," *Nonlinear Dyn.*, vol. 89, no. 2, pp. 1289–1308, 2017.

[2] L. Sun and Z. Zheng, "Disturbance observer-based robust saturated control for spacecraft proximity maneuvers," *IEEE Trans. Control Syst. Technol.*, vol. 26, no. 2, pp. 684–692, Mar. 2018.

[3] Y. Zou and W. Huo, "Singularity-free backstepping controller for model helicopters," *ISA Trans.*, vol. 65, pp. 133–142, Nov. 2016.

[4] X. Wang, Y. Chen, G. Lu, and Y. Zhong, "Robust flight control of small-scale unmanned helicopter," in *Proc. 32nd Chin. Control Conf.*, vol. 1, Jul. 2013, pp. 2700–2705.

[5] L. M. Belmonte, R. Morales, A. Fernández-Caballero, and J. A. Somolinos, "A tandem active disturbance rejection control for a laboratory helicopter with variable-speed rotors," *IEEE Trans. Ind. Electron.*, vol. 63, no. 10, pp. 6395–6406, Oct. 2016.

[6] M. He and J. He, "Extended state observer-based robust backstepping sliding mode control for a small-size helicopter," *IEEE Access*, vol. 6, pp. 33480–33488, 2018.

[7] M. He and J. He, "Modeling and robust attitude controller design for a small size helicopter," in *Proc. IEEE Int. Conf. Ind. Technol. (ICIT)*, Feb. 2019, pp. 145–150.

[8] R. E. Kalman, "A new approach to linear filtering and prediction problems," *ASME. J. Basic Eng.*, vol. 82, no. 1, pp. 35–45, 1960.

[9] C. Garriz and R. Domingo, "Development of trajectories through the Kalman algorithm and application to an industrial robot in the automotive industry," *IEEE Access*, vol. 7, pp. 23570–23578, 2019.
[10] N. J. Gordon, D. J. Salmond, and A. F. M. Smith, "Novel approach to nonlinear/non-Gaussian Bayesian state estimation," *IEE Proc. F, Radar Signal Process.*, vol. 140, no. 2, pp. 107–113, Apr. 1993.
[11] S. Julier, J. Uhlmann, and H. F. Durrant-Whyte, "A new method for the nonlinear transformation of means and covariances in filters and estimators," *IEEE Trans. Autom. Control*, vol. 45, no. 3, pp. 477–482, Mar. 2000.
[12] J.-J. Xiong and E.-H. Zheng, "Optimal Kalman filter for state estimation of a quadrotor UAV," *Optik*, vol. 126, no. 21, pp. 2862–2868, 2015.
[13] K. Ito and K. Xiong, "Gaussian filters for nonlinear filtering problems," *IEEE Trans. Autom. Control*, vol. 45, no. 5, pp. 910–927, May 2000.
[14] Q. Yang and L. Sun, "A fuzzy complementary Kalman filter based on visual and IMU data for UAV landing," *Optik*, vol. 173, pp. 279–291, Nov. 2018.
[15] B. Jia, M. Xin, and Y. Cheng, "Sparse-grid quadrature nonlinear filtering," *Automatica*, vol. 48, no. 2, pp. 327–341, 2012.
[16] J. Duník, O. Straka, and M. Šimandl, "Stochastic integration filter," *IEEE Trans. Autom. Control*, vol. 58, no. 6, pp. 1561–1566, Jun. 2013.
[17] I. Arasaratnam and S. Haykin, "Cubature Kalman filters," *IEEE Trans. Autom. Control*, vol. 54, no. 6, pp. 1254–1269, Jun. 2009.
[18] H. Benzerrouk, A. Nebylov, and H. Salhi, "Quadrotor UAV state estimation based on high-degree cubature Kalman filter," *IFAC-PapersOnLine*, vol. 49, no. 17, pp. 349–354, 2016.
[19] S.-H. Kim, L. Negash, and H.-L. Choi, "Cubature Kalman filter based fault detection and isolation for formation control of multi-UAVs," *IFAC-PapersOnLine*, vol. 49, no. 15, pp. 63–68, 2016.
[20] W. Huang, H. Xie, C. Shen, and J. Li, "A robust strong tracking cubature Kalman filter for spacecraft attitude estimation with quaternion constraint," *Acta Astron.*, vol. 121, pp. 153–163, Apr. 2016.
[21] K. P. B. Chandra, D.-W. Gu, and I. Postlethwaite, "Cubature Kalman filter based localization and mapping," *IFAC Proc. Volumes*, vol. 44, no. 1, pp. 2121–2125, 2011.
[22] C.-H. Tseng, S.-F. Lin, and D.-J. Jwo, "Fuzzy adaptive cubature Kalman filter for integrated navigation systems," *Sensors*, vol. 16, no. 8, pp. 1167–1189, 2016.
[23] H. Xiong, Z. Mai, J. Tang, and F. He, "Robust GPS/INS/DVL navigation and positioning method using adaptive federated strong tracking filter based on weighted least square principle," *IEEE Access*, vol. 7, pp. 26168–26178, 2019.
[24] H. Zhang, J. Xie, J. Ge, W. Lu, and B. Zong, "Adaptive strong tracking square-root cubature Kalman filter for maneuvering aircraft tracking," *IEEE Access*, vol. 6, pp. 10052–10061, 2018.
[25] H. Liu and W. Wu, "Strong tracking spherical simplex-radial cubature Kalman filter for maneuvering target tracking," *Sensors*, vol. 17, no. 4, p. 741, 2017.
[26] D. J. Jwo and S. H. Wang, "Adaptive fuzzy strong tracking extended Kalman filtering for GPS navigation," *IEEE Sensors J.*, vol. 7, no. 5, pp. 778–789, May 2007.
[27] B. Han, H. Huang, L. Lei, C. Huang, and Z. Zhang, "An improved IMM algorithm based on STSRCKF for maneuvering target tracking," *IEEE Access*, vol. 7, pp. 57795–57804, 2019.
[28] J. Wang, T. Zhang, X. Xu, and Y. Li, "A variational Bayesian based strong tracking interpolatory cubature Kalman filter for maneuvering target tracking," *IEEE Access*, vol. 6, pp. 52544–52560, 2018.
[29] D. Gebre-Egziabher, R. C. Hayward, and J. D. Powell, "Design of multi-sensor attitude determination systems," *IEEE Trans. Aerosp. Electron. Syst.*, vol. 40, no. 2, pp. 627–649, Apr. 2004.
[30] H. Miaolei and H. Jilin, "A real-time $H_\infty$ cubature Kalman filter based on SVD and its application to a small unmanned helicopter," *Optik*, vol. 140, pp. 96–103, Jul. 2017.